

Title	Germanium tin alloy nanowires as anode materials for high performance Li-ion batteries
Authors	Doherty, Jessica; McNulty, David; Biswas, Subhajt; Moore, Kalani; Conroy, Michele; Bangert, Ursel; O'Dwyer, Colm; Holmes, Justin D.
Publication date	43830
Original Citation	Doherty, J., McNulty, D., Biswas, S., Moore, K., Conroy, M., Bangert, U., O'Dwyer, C. and Holmes, J. D. (2020) 'Germanium tin alloy nanowires as anode materials for high performance Li-ion batteries', <i>Nanotechnology</i> , 31(16), 165402 (9 pp). doi: 10.1088/1361-6528/ab6678
Type of publication	Article (peer-reviewed)
Link to publisher's version	https://iopscience.iop.org/article/10.1088/1361-6528/ab6678 - 10.1088/1361-6528/ab6678
Rights	© 2020 IOP Publishing Ltd. This Accepted Manuscript is available for reuse under a CC BY-NC-ND 3.0 licence after a 12 month embargo period. After the embargo period, everyone is permitted to use, copy and redistribute this article for non-commercial purposes only, provided that they adhere to all the terms of the licence https://creativecommons.org/licenses/by-nc-nd/3.0 - https://creativecommons.org/licenses/by-nc-nd/4.0/
Download date	2025-07-03 23:37:50
Item downloaded from	https://hdl.handle.net/10468/9479



UCC

University College Cork, Ireland
Coláiste na hOllscoile Corcaigh

ACCEPTED MANUSCRIPT

Germanium Tin Alloy Nanowires as Anode Materials for High Performance Li-Ion Batteries

To cite this article before publication: Jessica Doherty *et al* 2019 *Nanotechnology* in press <https://doi.org/10.1088/1361-6528/ab6678>

Manuscript version: Accepted Manuscript

Accepted Manuscript is “the version of the article accepted for publication including all changes made as a result of the peer review process, and which may also include the addition to the article by IOP Publishing of a header, an article ID, a cover sheet and/or an ‘Accepted Manuscript’ watermark, but excluding any other editing, typesetting or other changes made by IOP Publishing and/or its licensors”

This Accepted Manuscript is © 2019 IOP Publishing Ltd.

During the embargo period (the 12 month period from the publication of the Version of Record of this article), the Accepted Manuscript is fully protected by copyright and cannot be reused or reposted elsewhere.

As the Version of Record of this article is going to be / has been published on a subscription basis, this Accepted Manuscript is available for reuse under a CC BY-NC-ND 3.0 licence after the 12 month embargo period.

After the embargo period, everyone is permitted to use copy and redistribute this article for non-commercial purposes only, provided that they adhere to all the terms of the licence <https://creativecommons.org/licenses/by-nc-nd/3.0>

Although reasonable endeavours have been taken to obtain all necessary permissions from third parties to include their copyrighted content within this article, their full citation and copyright line may not be present in this Accepted Manuscript version. Before using any content from this article, please refer to the Version of Record on IOPscience once published for full citation and copyright details, as permissions will likely be required. All third party content is fully copyright protected, unless specifically stated otherwise in the figure caption in the Version of Record.

View the [article online](#) for updates and enhancements.

Germanium Tin Alloy Nanowires as Anode Materials for High Performance Li-Ion Batteries

Jessica Doherty^{1,2}, David McNulty¹, Subhajit Biswas^{1,2}, Kalani Moore³, Michele Conroy³, Ursel Bangert³, Colm O'Dwyer¹ and Justin D. Holmes^{1,2*}*

School of Chemistry, ERI and Tyndall National Institute, University College Cork, Cork, T12 YN60, Ireland. ²AMBER@CRANN, Trinity College Dublin, Dublin 2, Ireland. ³Department of Physics, Bernal Institute, University of Limerick.

*Author to whom correspondence should be addressed: Tel: +353 (0)21 4903608; Fax: +353 (0)21 4274097; E-mail: j.holmes@ucc.ie (JDH) and s.biswas@ucc.ie (SB)

1
2
3 ABSTRACT: The combination of two active Li-ion materials (Ge and Sn) can result in
4 improved conduction paths and higher capacity retention. Here we report; for the first time;
5
6 the implementation of $\text{Ge}_{1-x}\text{Sn}_x$ alloy nanowires as anode materials for Li-ion batteries. Ge_{1-x}
7
8 Sn_x alloy nanowires have been successfully grown via vapor-liquid-solid (VLS) technique
9
10 directly on stainless steel current collectors. $\text{Ge}_{1-x}\text{Sn}_x$ ($x = 0.048$) nanowires were
11
12 predominantly seeded from the $\text{Au}_{0.80}\text{Ag}_{0.20}$ catalysts with negligible amount of growth was
13
14 also directly catalysed from stainless steel substrate. The electrochemical performance of the
15
16 the $\text{Ge}_{1-x}\text{Sn}_x$ nanowires as an anode material for Li-ion batteries was investigated via
17
18 galvanostatic cycling and detailed analysis of differential capacity plots. The nanowire
19
20 electrodes demonstrated an exceptional capacity retention of 93.4 % from the 2nd to the 100th
21
22 charge at a C/5 rate, while maintaining a specific capacity value of ~921 mAh/g after 100
23
24 cycles. Voltage profiles and differential capacity plots revealed that the $\text{Ge}_{1-x}\text{Sn}_x$ nanowires
25
26 behave as an alloying mode anode material, as reduction/oxidation peaks for both Ge and Sn
27
28 were observed, however it is clear that the reversible lithiation of Ge is responsible for the
29
30 majority of the charge stored.
31
32
33
34
35
36
37
38
39
40

41 **Keywords:** Nanowire; GeSn alloy; Li-ion battery;
42
43
44
45
46
47
48
49
50
51
52
53
54
55
56
57
58
59
60

1. Introduction

Advancement in Li-ion batteries requires the availability of scalable, cost-effective materials with high energy density.[1] Despite its relatively low capacity (372 mAh/g), graphite remains to be the most commonly used anode material for Li-ion batteries.[2] Other group IV materials, such as Si, Ge and Sn, exhibit bulk capacities far in excess of those of graphite (3579 mAh/g, 1620 mAh/g, , 991 mAh/g respectively),[3] however, due to the enormous expansion of bulk Ge and Si upon lithiation, leading to the pulverisation of the material, the cycle life, and thus retention of the material, is decreased. Nanowires offer a unique solution to this problem; the ability of nanowires to transition from crystalline to amorphous phase while retaining their structural integrity make them suitable materials for use in Li-ion batteries. Hence, the manufacturing of group IV nanowires for use as battery materials has been widely explored.[3–6] Ge nanowires in particular have been identified for their suitability as anode materials in Li-ion batteries.[2,7–10] Both Sn and Pb-catalysed Ge nanowires have previously been reported to demonstrate high capacities when used as an anode material for Li ion batteries[11], however there are no reports on the effect of the incorporation of Sn in the Ge nanowire lattice on the performance of Li-ion battery.

Ge shows enhanced battery performance over its group IV counterparts, Si and Sn, and increased carrier mobility.[12] However, Ge also demonstrates poor cycling life and capacity fading. With its high electronic conductivities and theoretical capacity, Sn is a good candidate for alloying with Ge for energy storage applications.[13] The combination of two active Li-ion materials can result in improved conduction paths with higher capacity retention[14] due to different level of expansion of Ge and Sn component in the alloy with lithiation.[15] The use of a $\text{Ge}_{1-x}\text{Sn}_x$ alloys has previously been shown to enhance the energy storage properties of

1
2
3 Ge in nanocrystal and amorphous form.[12–14] $\text{Ge}_{1-x}\text{Sn}_x$ nanocrystals with $x = 0.05$ showed
4 an improvement in capacitance and retention over Ge nanocrystals.[12] However, the surface
5 area of these nanomaterials is too high, leading to significant side reactions.[14] The open
6 continuous channel along the axis of a nanowire, on the other hand, could result in an increase
7 in capacity and retention due to a decrease in sidewall reactions.[16] Further to this, relative
8 cost of the Ge anode materials could be also reduced by alloying it with the cheaper and more
9 abundant Sn. Therefore, we report the fabrication of $\text{Ge}_{1-x}\text{Sn}_x$ alloy nanowires using AuAg
10 alloy nanoparticle catalyst, which are grown directly on stainless steel current collector for use
11 as anode materials in Li-ion batteries. The growth of $\text{Ge}_{1-x}\text{Sn}_x$ nanowires directly on the
12 stainless steel current collector eliminates the requirement to prepare a conductive slurry of the
13 active material with a binder. The high capacities ($> 900 \text{ mAh/g}$ after 100 cycles) and
14 impressive capacity retention verify the potential of our binder-free $\text{Ge}_{1-x}\text{Sn}_x$ nanowire
15 electrodes as promising anode materials.
16
17
18
19
20
21
22
23
24
25
26
27
28
29
30
31
32
33
34
35
36

37 2. Method

38
39
40 **Nanowire fabrication process:** For the catalyzation of $\text{Ge}_{1-x}\text{Sn}_x$ nanowires in a three phase
41 bottom-up growth dodecanethiol-stabilized, phase pure, $\text{Au}_{0.80}\text{Ag}_{0.20}$ alloy nanoparticles were
42 used. Colloidal nanoparticles were synthesized by co-reducing a mixture of chloroauric acid
43 (HAuCl_4) and silver nitrate (AgNO_3) in a chloroform/water biphasic solution.[22,24,40,41]
44 These metal nanoparticles were deposited on to a stainless steel substrate via spin coating. A
45 metal reaction vessel containing the nanoparticle-coated substrate was then left under vacuum
46 at $180 \text{ }^\circ\text{C}$ for 12 hr to ensure a moisture-free growth atmosphere and the desorption of the
47 surfactant molecules from the nanoparticle catalysts.
48
49
50
51
52
53
54
55
56
57
58
59
60

1
2
3 The Ge and Sn sources used were diphenylgermane (DPG) and tetraethyltin (TET)
4 respectively. These precursors were dissolved in anhydrous toluene (10 ml) in an N₂ filled
5 glove box with typical Ge and Sn precursor volumes of 0.025 ml and 0.0045 ml respectively.
6
7
8
9
10 A solution containing both Ge and Sn precursors was loaded into a Hamilton sample-lock
11 syringe inside the nitrogen-filled glovebox.
12
13
14

15
16
17 Au_{0.80}Ag_{0.20}-coated stainless steel substrate was further annealed for 15 min at 440 °C under a
18 flowing H₂/Ar atmosphere inside a tube furnace prior to the injection of precursors. The
19 precursor solution was then injected into the metal reaction vessel using a syringe pump at a
20 rate of 0.025 ml min⁻¹. A H₂/Ar flow rate of 0.6 sccm was maintained during the entire growth
21 period. Various growth times were employed to determine the growth rate, ranging from 15 –
22
23
24
25
26
27
28
29
30
31
32
33
34
35
36
37
38
39
40
41
42
43
44
45
46
47
48
49
50
51
52
53
54
55
56
57
58
59
60

120 min.

Characterization of nanowires: Bottom-up grown Ge_{1-x}Sn_x nanowires were imaged on a FEI
Helios NanoLab 600i scanning electron microscope (SEM). All energy-dispersive X-ray
(EDX) measurements were recorded in high-angle annular dark-field mode in the FEI Helios
NanoLab 600i operating at 30 kV and 0.69 nA with an attached Oxford X-Max 80 detector.
Error in the EDX measurements indicates a standard error of 0.5 at. %. HRTEM imaging was
performed in Titan Themis transmission electron microscope.

Characterization of nanowires as anode in Li-ion battery: The electrochemical performance
of the nanowires is evaluated on the stainless steel substrate which also functions as a current
collector. As they are grown on the stainless steel they are quite well adhered to the substrate.
One of the novel aspects of the electrodes is that they do not have to add any additional
processing steps, for example preparation of a slurry consisting of our nanowires with a

1
2
3
4
5
6
7
8
9
10
11
12
13
14
15
16
17
18
19
20
21
22
23
24
25
26
27
28
29
30
31
32
33
34
35
36
37
38
39
40
41
42
43
44
45
46
47
48
49
50
51
52
53
54
55
56
57
58
59
60

conductive additive and a binder. Electrochemical measurements were performed using a BioLogic VSP Potentiostat/Galvanostat. The electrochemical properties of $\text{Ge}_{1-x}\text{Sn}_x$ nanowire samples were investigated in a half cell configuration against a pure Li counter electrode in a two electrode, stainless steel split cell (a coin cell assembly that can be disassembled for post-mortem analysis). The electrolyte used consisted of a 1 mol dm^{-3} solution of lithium hexafluorophosphate salt in a 1:1 (v/v) mixture of ethylene carbonate in dimethyl carbonate with 3 wt% vinylene carbonate. The separator used was a glass fiber separator (El-Cell ECC1-01-0012-A/L, 18 mm diameter, 0.65 mm thickness). The mass loading for anode samples was $\sim 0.3 \text{ mg per } 0.5 \text{ cm}^2$ and no additional conductive additives or binders were added. A Mettler Toledo XP2U ultra micro balance was used to determine the mass of $\text{Ge}_{1-x}\text{Sn}_x$ nanowire material on the stainless steel substrates. Galvanostatic cycling was performed at 0.2 C in a potential window of 1.5 – 0.01 V (vs Li/Li⁺).

3. Results & Discussion

The direct growth of $\text{Ge}_{1-x}\text{Sn}_x$ nanostructures on a stainless steel substrate for use as anode material for Li-ion batteries presents a new venture in the growth of $\text{Ge}_{1-x}\text{Sn}_x$ nanowires, and to our knowledge, this study represents the first reported instance of $\text{Ge}_{1-x}\text{Sn}_x$ alloy nanowires for use in Li-ion batteries. Nanowire growth was carried out via a bottom-up method using diphenylgermane (DPG) and tetraethyltin (TET) as the Ge and Sn sources respectively, and $\text{Au}_{0.80}\text{Ag}_{0.20}$ nanoparticles as the growth catalysts.[17] A liquid-injection CVD approach was adapted for the growth of nanowires at 440 °C on stainless steel current collector substrate. A scanning electron microscopy (SEM) image of $\text{Ge}_{1-x}\text{Sn}_x$ nanowires grown on stainless steel is presented in Figure 1(a). The nanowires have a mean diameter of $75 \pm 30 \text{ nm}$. Low resolution STEM imaging (Figure 1(b)) reveals bright contrasted spherical nanoparticles at the tips of the

1
2
3 nanowires and negligible tapering of nanowire along their lengths. Energy dispersive X-ray
4 (EDX) analysis of the $\text{Ge}_{1-x}\text{Sn}_x$ nanowires revealed an average Sn content of 4.8 ± 2.1 at. %.
5
6 This Sn incorporation was consistent throughout the nanowire body; without considering the
7 spherical tip, both radially and axially, as verified by EDX elemental mapping (Figure 1(c)).
8
9 EDX mapping also revealed the formation of a Sn-rich alloy at the tips of the nanowires at a
10
11 growth temperature of 440°C (Figure 1(c)).
12
13
14
15
16
17
18
19
20

21 However, the use of a stainless steel substrate did alter the quality of the grown nanowires, in
22 terms of morphology and Sn content, compared to $\text{Ge}_{1-x}\text{Sn}_x$ nanowires previously grown on Si
23 substrates under similar growth constrains [17,18]. These differences could possibly be due to
24 the difference in the surface energies of the Si and stainless steel substrates which result in
25 different wetting and surface curvatures of the intermediate eutectic liquid (AuAg-Sn-Ge in
26 this case) during VLS growth. Differences in the curvature of the liquid eutectic can readily
27 influence the absorption of growth species and growth kinetics at different interfaces (vapor-
28 liquid, liquid-solid *etc.*), thus resulting in $\text{Ge}_{1-x}\text{Sn}_x$ nanowires with different morphologies.
29
30 Further to this, the incorporation of Sn in Ge is aided by “solute trapping” of Sn impurities
31 which could be influenced by the growth kinetics, interfacial geometry and strain at different
32 interface.[17,18] Thus a different Sn incorporation in the GeSn alloy nanowires is observed
33 for stainless steel substrates compared to Si growth substrate. Additionally, the possible
34 participation of iron-based catalysts as additional growth promoters[19] from the stainless steel
35 substrate may also have resulted in a vapor-solid-solid (VSS)-like nanowire growth regime,
36 thus resulting in wider diameter distribution of nanowire (Supporting Info, Figure S1). The
37 large variation in the Sn content (4.8 ± 2.1 at. %) in the $\text{Ge}_{1-x}\text{Sn}_x$ nanowire sample can be
38 attributed to the two competing growth regimes present with the participation of two different
39
40
41
42
43
44
45
46
47
48
49
50
51
52
53
54
55
56
57
58
59
60

1
2
3 growth promoters. Analysis of the catalyst seed at the nanowire tips also revealed two distinct
4
5 compositions, Fe rich Fe/Ge/Sn and Sn rich Au/Ag/Ge/Sn (Figure 1(d) and (e)). The Ge/Fe
6
7 rich nanowire tips had a composition of approximately 65 at. % Fe and 35 at. % Ge with
8
9 minimal Sn incorporation (~ 3 at. %). These Fe₂Ge catalysed VSS like growth resulted in Sn
10
11 deficient (≈ 1 at.%) Ge_{1-x}Sn_x nanowires (Figure S2 in Supporting Information). Alternatively,
12
13 Ge_{1-x}Sn_x nanowires with Sn rich tips, containing Au and Ag, contained a higher Sn amount ($>$
14
15 5 at. %). By analysing the nanowire tips (approximately 50 nanowires), it was found that
16
17 statistically ~ 75 % of the nanowires were seeded by Au/Ag/Sn seed with high Sn. Fe-seeded
18
19 nanowires accounted for a minority of the Ge_{1-x}Sn_x nanowires grown. The lower Sn
20
21 composition (~ 1 at. %) in the Ge_{1-x}Sn_x nanowires (Supporting Info, Figure S2) seeded directly
22
23 from stainless steel substrate is expected due to the VSS nature of the Fe seeded Ge_{1-x}Sn_x
24
25 growth; the eutectic temperatures of Fe-Ge[20] and Fe-Sn[21] are far above the growth
26
27 temperature of the Ge_{1-x}Sn_x nanowires. As Sn incorporation is likely aided by a solute trapping
28
29 mechanism,[17,22] participation and formation of a Fe-Ge-Sn based stable alloy solid growth
30
31 seeds with very low Sn content does not encourage incorporation and trapping of Sn impurities
32
33 at the seed-nanowire interface. Interestingly, in the Fe-seeded Ge_{1-x}Sn_x nanowires, Sn was still
34
35 present in non-trivial amounts in the majority of the nanowires (Supporting Info, Figure S2).
36
37 However, as both of these nanowire types; catalysed from stainless steel and AuAg alloy seeds;
38
39 contribute as anode materials in Li-ion batteries to the overall capacitance and cycle life, both
40
41 types of Ge_{1-x}Sn_x nanowire were included in the determination of the average Sn composition.
42
43
44
45
46
47
48
49
50
51
52 High resolution scanning transmission electron microscopy (HRSTEM) of the Au_{0.80}Ag_{0.20}-
53
54 seeded Ge_{1-x}Sn_x nanowires ($x = 0.048$) revealed the highly crystalline nature of the nanowires
55
56 with sharp seed/nanowire interfaces (Figure 2). Figure 2(a) depicts the bright field HRSTEM
57
58 image of a defect free, single crystalline Ge_{1-x}Sn_x nanowires. As defect free materials allow
59
60

1
2
3 for a long life cycles, the structural uniformity of the $\text{Ge}_{1-x}\text{Sn}_x$ nanowires is imperative for their
4 use as Li ion anode materials.[23] Fast Fourier Transform (FFT) analysis of the nanowire, with
5 $\langle 110 \rangle$ zone axis alignment (Figure 2(a) inset), revealed an interplanar spacing (d) of 0.33 nm,
6 which is marginally larger than the d value for bulk diamond Ge crystals of 0.326 nm (JCPDS
7 04–0545). The d spacing is expected to increase upon the incorporation of Sn into the Ge host
8 lattice due to the difference in the lattice constants of Ge and Sn, which can instigate a lattice
9 expansion, and has been previously reported.[22] The nanowires predominantly displayed a
10 $\langle 111 \rangle$ growth direction, the most common growth orientation for Ge nanowires with a mean
11 diameter above 50 nm[22,24]. Generally, the crystal structure of the $\text{Ge}_{1-x}\text{Sn}_x$ alloy nanowires,
12 with various Sn incorporations, exhibited a 3C lattice arrangement without any stacking faults
13 and twin boundaries. The interface between the nanowire seed and body was examined and
14 can be seen in Figure 2(b). No apparent tailing or segregation of Sn from the Sn rich seed was
15 observed, confirming the sharp junction at the interface as indicated from the EDX elemental
16 maps in Figure 1(c). The interplanar spacing of the nanowire seed (d) was 0.28 nm, confirmed
17 by measurement of the lattice spacing for multiple layers. The interplanar spacing and FFT of
18 a nanowire seed (Figure 2(b), inset) matches well with tetragonal Sn (JCPDS 04–0673),
19 confirming the Sn-rich nature of the nanowire seed.
20
21
22
23
24
25
26
27
28
29
30
31
32
33
34
35
36
37
38
39
40
41
42
43
44
45

46 The electrochemical performance of the $\text{Ge}_{1-x}\text{Sn}_x$ nanowires as an anode material for Li-ion
47 batteries was investigated via galvanostatic cycling in a half-cell configuration versus Li metal.
48 A selection of the charge and discharge voltage profiles obtained from galvanostatic cycling
49 using a C/5 rate are shown in Figure 3(a) and (b). The first charge curve consisted of a sloping
50 region from an open circuit voltage (OCV) (3.20 V) to ~ 0.35 V, followed by a long plateau
51 from ~ 0.30 V to the low potential limit of 0.01 V. The sloping region is associated with the
52 formation of a solid-electrolyte interphase (SEI) layer and the irreversible decomposition of
53
54
55
56
57
58
59
60

1
2
3 the electrolyte on the surface of the $\text{Ge}_{1-x}\text{Sn}_x$ nanowires.[25] The plateau is attributed to the
4 alloying of the nanowires with Li.[26] The first discharge curve consisted of a plateau at ~ 0.50
5 V, corresponding to the dealloying of the $\text{Ge}_{1-x}\text{Sn}_x$ nanowires. The initial charge and discharge
6 capacities were ~ 1716 and 867 mAh/g, respectively, corresponding to an initial Coulombic
7 efficiency (ICE) of 50.5 %. The large initial charge capacity is likely due to the formation of
8 an SEI layer on the surface of the nanowires as well as the formation of quasi reversible
9 Li_2O .[27] The ICE value obtained for $\text{Ge}_{1-x}\text{Sn}_x$ nanowires is comparable to or greater than ICE
10 values reported for other Ge nanowire anodes.[7,28] Low ICE is a persistent issue for alloying
11 mode anode materials such as Ge and Si based negative electrode materials however, there are
12 some reports demonstrating that the prelithiation of Si nanostructures can improve ICE values.
13 Forney et al. prelithiated Si-CNT anodes via mechanical pressing of stabilized lithium metal
14 powder onto the working electrode, and demonstrated a significant increase in ICE values.[29]
15 The voltage profiles from the 2nd cycle to the 100th cycle are quite consistent, which is
16 indicative of a highly reversible process.

17
18
19
20
21
22
23
24
25
26
27
28
29
30
31
32
33
34
35
36
37
38
39 $\text{Ge}_{1-x}\text{Sn}_x$ nanowires has potential to demonstrate stable capacity retention due to lower volume
40 expansion (305%) of Sn compared to Ge (382%).[15] The specific capacity values obtained
41 over 100 cycles at a rate of C/5 and the corresponding coulombic efficiencies are shown in
42 Figure 3(c). The specific capacity after the 2nd charge was ~ 986 mAh/g and after 100 cycles
43 this decreased marginally to ~ 921 mAh/g, corresponding to an exceptional capacity retention
44 of 93.4 %. The average Coulombic efficiency from the 2nd to the 100th cycle was also
45 impressive, having a value of 97.8 %. Preserving such a high level of capacity after 100 cycles
46 clearly validates the viability of $\text{Ge}_{1-x}\text{Sn}_x$ nanowires for use as an anode material in practical
47 commercial Li-ion cells. The specific capacity values achieved for the $\text{Ge}_{1-x}\text{Sn}_x$ nanowires are
48 comparable to [11,30] or greater than [31–34] previously reported values for other Ge based
49
50
51
52
53
54
55
56
57
58
59
60

1
2
3 anode materials. Notably, the impressive electrochemical performance of the GeSn nanowires
4 was achieved without the need of conductive additives or binders.
5
6
7
8
9

10
11 In order to better appreciate the charge storage mechanism of the $\text{Ge}_{1-x}\text{Sn}_x$ nanowires, which
12 results in their impressive capacity retention properties, differential capacity plots from
13 galvanostatic charge and discharge curves were calculated. The initial charge curve consisted
14 of a series of plateaus which can be seen more clearly in the differential capacity plot (DCP)
15 presented in Figure S3(a). The DCP for the first charge consisted of 5 peaks in total. The wide
16 band centred at ~ 1.21 V is associated with the formation of an SEI layer and is only observed
17 during the first cycle.[35] The weak peak present at ~ 0.74 V may be attributed to the alloying
18 of Li with the low amount of Sn (4.8 at. % Sn) which is present in the nanowires. A reduction
19 peak at this potential has previously been reported for Sn-based anode materials.[30] The
20 strong, sharp peak centred at 0.35 V is due to the due to the lithiation of crystalline Ge (c-Ge)
21 and is only observed during the first cycle, suggesting that after the initial lithiation of the
22 nanowires, they do not return to a fully delithiated crystalline Ge phase. A similar observation
23 for this reduction peak was made by Mullane et al. for Cu-catalysed Ge nanowires.[2] The
24 strong peak at 0.19 V and the weaker shoulder at 0.15 V are due to the initial formation of Li-
25 Ge alloys in the form of a- $\text{Li}_{15}\text{Ge}_4$ and c- $\text{Li}_{15}\text{Ge}_4$, respectively.[30] A strong, wide, asymmetric
26 oxidation peak was observed in the first cathodic scan from 0.35 to 0.55 V, which can be
27 deconvoluted into two distinct peaks centred at 0.49 and 0.51 V, as shown in Figure S3(c),
28 corresponding to the delithiation of the c- $\text{Li}_{15}\text{Ge}_4$ and a- $\text{Li}_{15}\text{Ge}_4$ phases, respectively.[36,37]
29
30
31
32
33
34
35
36
37
38
39
40
41
42
43
44
45
46
47
48
49
50
51

52
53
54
55
56 The DCP for the 2nd charge consisted of two wide peaks centred at 0.53 and 0.39 V and a sharp
57 peak at 0.18 V (Figure S3(d)). The two broad peaks are associated with the formation of
58
59
60

1
2
3 amorphous Li-Ge alloys ($a\text{-Li}_x\text{Ge} \rightarrow a\text{-Li}_{15}\text{Ge}_4$) and the sharp peak is due to the formation of
4 $c\text{-Li}_{15}\text{Ge}_4$. [10,38] Contour plots, calculated from a series of DCPs from charge and discharge
5 voltage profiles, ranging from the 2nd to the 100th cycle are shown in Figure 4. The reduction
6 peaks associated with the formation of the $a\text{-Li}_{15}\text{Ge}_4$ and $c\text{-Li}_{15}\text{Ge}_4$ phases, centred at 0.39 and
7 0.18 V, remain present during the 100 cycles, as shown in Figure 4a. This indicates highly
8 reversible lithiation/delithiation of $\text{Ge}_{1-x}\text{Sn}_x$ nanowires. The presence of these reduction peaks
9 and the consistency of the potentials at which they occur is a major contributing factor to the
10 impressive capacity retention of the nanowires from the 2nd cycle onwards. Initially the
11 majority of the charge stored by the $\text{Ge}_{1-x}\text{Sn}_x$ nanowires is due to the formation of the $c\text{-Li}_{15}\text{Ge}_4$
12 phase, as indicated by the red area in Figure 4a, however as cycling continues the intensity of
13 this reduction peak decreases slightly while the intensity of the reduction peak associated with
14 the formation of the $a\text{-Li}_{15}\text{Ge}_4$ phase remains consistent. This suggests that with increased
15 cycling more of the charge stored is due to the transition from $a\text{-Li}_x\text{Ge} \rightarrow a\text{-Li}_{15}\text{Ge}_4$.

16
17
18
19
20
21
22
23
24
25
26
27
28
29
30
31
32
33
34
35
36 The contour plot calculated from the DCPs for discharge curves is shown in Figure 4d. The
37 asymmetric oxidation peak associated with the delithiation of the $c\text{-Li}_{15}\text{Ge}_4$ and $a\text{-Li}_{15}\text{Ge}_4$
38 phases remains after 100 cycles, however there is a significant decrease in the intensity after
39 the first 30 cycles. The stacked DCPs in Figures 4e and f indicate that the width of the peak
40 increases with increased cycling, which may be associated with decreased charge storage due
41 to the formation of the $c\text{-Li}_{15}\text{Ge}_4$ phase. Of note, the discharge capacity values presented in
42 Figure 4c do not significantly decrease after 30 cycles, hence the widening of this oxidation
43 peak with increased cycling does not have a substantial negative influence on the overall charge
44 stored. Initially the majority charge storage mechanism for the $\text{Ge}_{1-x}\text{Sn}_x$ nanowires is the
45 formation of the $c\text{-Li}_{15}\text{Ge}_4$ phase, however as cycling continues, less charge is being stored via
46 the formation of this phase and more of the overall charge stored is due to the formation of the
47
48
49
50
51
52
53
54
55
56
57
58
59
60

1
2
3 a-Li₁₅Ge₄ phase. We have previously observed a similar trend for GeO₂ inverse opal structured
4
5 anodes, whereby after a number of cycles the preferred charge storage mechanism was the
6
7 formation of the a-Li₁₅Ge₄ phase rather than the c-Li₁₅Ge₄ phase.[39] Deformation and
8
9 electrochemical restructuring of nanowire morphology and amorphization of the GeSn
10
11 material; similar to Ge nanowires [30]; was observed after 100 cycles (Figure S4 in Supporting
12
13 Information). Formation of a mesh of active material by agglomeration of individual nanowires
14
15 was observed for phase pure Ge nanowire after 100 cycles. [30] A very similar behavior was
16
17 observed for the GeSn nanowires where a porous network of active material with ligament and
18
19 mesh like morphology is formed after 100 cycles. Actually, compared to the phase pure Ge
20
21 nanowire these GeSn nanowire shows better retention of nanowire morphology with the
22
23 withholding of the cylindrical shape after 100 cycles (Figure S4), though other factors such as
24
25 dimension, cycling rate, anode fabrication method etc. may affect this transformation.
26
27 Retention of the alloy structure is also confirmed from the corresponding EDX mapping
28
29 (Figure S4) with no apparent sign of phase segregation of Ge or Sn in the cycled structure.
30
31
32
33
34
35
36
37
38

39 4. CONCLUSION

40
41
42 Ge_{1-x}Sn_x alloy nanowires were successfully grown directly on stainless steel substrates, current
43
44 collectors for Li-ion battery, thus eliminating the requirement to prepare a conductive slurry of
45
46 the active material with a binder. Ge_{1-x}Sn_x nanowires with $x \approx 0.048$ were determined to be
47
48 seeded both from the Au_{0.80}Ag_{0.20} nanoparticle catalyst and from the substrate itself (Fe). The
49
50 Ge_{1-x}Sn_x nanowires were single crystalline and defect free prior to lithiation. The
51
52 electrochemical performance of the the Ge_{1-x}Sn_x nanowires as an anode material for Li-ion
53
54 batteries was investigated via galvanostatic cycling. The nanowire electrodes demonstrated an
55
56 exceptional capacity retention of 93.4 % from the 2nd to the 100th charge at a C/5 rate, while
57
58
59
60

1
2
3 maintaining a specific capacity value of ~921 mAh/g after 100 cycles. Voltage profiles and
4
5 differential capacity plots revealed that the $\text{Ge}_{1-x}\text{Sn}_x$ nanowires behaved as a dual alloying mode
6
7 anode material as reduction/oxidation peaks for both Ge and Sn were observed. However, it
8
9 was clear that the reversible lithiation of Ge was responsible for the majority of the charge
10
11 stored due to the relatively low amount of Sn present within the alloy nanowires (4.8 at. % Sn).
12
13 A future goal would be to find the Sn based group IV binary and ternary (including Si) alloy
14
15 nanomaterials with critical composition as the highly efficient anode material for Li-ion
16
17 battery.
18
19
20
21
22
23
24

25 **Supporting Information**

26
27
28 The Supporting Information is available from IOP.

29
30
31 Supporting Information content experimental method, diameter distribution, EDX spectra and
32
33 differential charge curves and STEM images of cycled material.
34
35
36
37
38
39

40 **Acknowledgements**

41
42
43 This research was funded by Science Foundation Ireland (Grant No: 14/IA/2513), and by the
44
45 Irish Research Council through a Postgraduate Scholarship to JD (Grant No.:
46
47 GOIPG/2015/2772).
48
49
50
51

52 **Conflict of Interest**

53
54 The authors declare no competing financial interest.
55
56
57
58
59
60

REFERENCES

- [1] Osiak M, Geaney H, Armstrong E and O'Dwyer C 2014 Structuring materials for lithium-ion batteries: Advancements in nanomaterial structure, composition, and defined assembly on cell performance *J. Mater. Chem. A* **2** 9433–60
- [2] Mullane E, Kennedy T, Geaney H and Ryan K M 2014 A rapid, solvent-free protocol for the synthesis of germanium nanowire lithium-ion anodes with a long cycle life and high rate capability *ACS Appl. Mater. Interfaces* **6** 18800–7
- [3] Tian H, Xin F, Wang X, He W and Han W 2015 High capacity group-IV elements (Si, Ge, Sn) based anodes for lithium-ion batteries *J. Mater.* **1** 153–69
- [4] Bogart T D, Chockla A M and Korgel B A 2013 High capacity lithium ion battery anodes of silicon and germanium *Curr. Opin. Chem. Eng.* **2** 286–93
- [5] Stokes K, Geaney H, Flynn G, Sheehan M, Kennedy T and Ryan K M 2017 Direct Synthesis of Alloyed Si $1-x$ Ge x Nanowires for Performance-Tunable Lithium Ion Battery Anodes *ACS Nano* **11** 10088–96
- [6] Kennedy T, Brandon M and Ryan K M 2016 Advances in the Application of Silicon and Germanium Nanowires for High-Performance Lithium-Ion Batteries *Adv. Mater.*
- [7] Chockla A M, Klavetter K C, Mullins C B and Korgel B A 2012 Solution-grown germanium nanowire anodes for lithium-ion batteries *ACS Appl. Mater. Interfaces* **4** 4658–64
- [8] Flynn G, Palaniappan K, Sheehan M, Kennedy T and Ryan K M 2017 Solution synthesis of lead seeded germanium nanowires and branched nanowire networks and their application as Li-ion battery anodes *Nanotechnology* **28**
- [9] Li X, Yang Z, Fu Y, Qiao L, Li D, Yue H and He D 2015 Germanium anode with

- 1
2
3 excellent lithium storage performance in a germanium/lithium-cobalt oxide lithium-ion
4 battery *ACS Nano* **9** 1858–67
5
6
7
8
9 [10] Liu X H, Huang S, Picraux S T, Li J, Zhu T and Huang J Y 2011 Reversible nanopore
10 formation in Ge nanowires during lithiation- delithiation cycling: An in situ transmission
11 electron microscopy study *Nano Lett.* **11** 3991–7
12
13
14
15 [11] Mullane E, Kennedy T, Geaney H, Dickinson C and Ryan K M 2013 Synthesis of tin
16 catalyzed silicon and germanium nanowires in a solvent-vapor system and optimization
17 of the seed/nanowire interface for dual lithium cycling *Chem. Mater.* **25** 1816–22
18
19
20
21 [12] Cho Y J, Kim C H, Im H S, Myung Y, Kim H S, Back S H, Lim Y R, Jung C S, Jang
22 D M, Park J, Lim S H, Cha E H, Bae K Y, Song M S and Cho W Il 2013 Germanium-
23 tin alloy nanocrystals for high-performance lithium ion batteries *Phys. Chem. Chem.*
24 *Phys.* **15** 11691–5
25
26
27
28
29
30
31
32
33 [13] Lee H and Cho J 2007 Sn₇₈Ge₂₂@carbon core-shell nanowires as fast and high-
34 capacity lithium storage media *Nano Lett.* **7** 2638–41
35
36
37
38
39 [14] Kim M G and Cho J 2009 Nanocomposite of Amorphous Ge and Sn Nanoparticles as
40 an Anode Material for Li Secondary Battery *J. Electrochem. Soc.* **156** A277
41
42
43
44 [15] Chou C, Kim H and Hwang G S 2011 A Comparative First-Principles Study of the
45 Structure , Energetics , and Properties of Li À M (M = Si , Ge , Sn) Alloys 20018–26
46
47
48
49 [16] Yang Z, Du G, Meng Q, Guo Z, Yu X, Chen Z, Guo T and Zeng R 2011 Dispersion of
50 SnO₂ nanocrystals on TiO₂(B) nanowires as anode material for lithium ion battery
51 applications *RSC Adv.* **1** 1834
52
53
54
55
56
57 [17] Doherty J, Biswas S, Saladukha D, Ramasse Q, Bhattacharya T S, Singha A, Ochalski
58 T J and Holmes J D 2018 Influence of growth kinetics on Sn incorporation in direct band
59
60

- 1
2
3 gap Ge_{1-x}Sn_x nanowires *J. Mater. Chem. C* 8738–50
4
5
6 [18] Biswas S, Doherty J, Saladukha D, Ramasse Q, Majumdar D, Upmanyu M, Singha A,
7 Ochalski T, Morris M A and Holmes J D 2016 Non-equilibrium induction of tin in
8 germanium: Towards direct bandgap Ge_{1-x}Sn_xnanowires *Nat. Commun.* **7**
9
10
11
12
13 [19] Biswas S, Doherty J, Majumdar D, Ghoshal T, Rahme K, Conroy M, Singha A, Morris
14 M A and Holmes J D 2015 Diameter-controlled germanium nanowires with lamellar
15 twinning and polytypes *Chem. Mater.* **27**
16
17
18
19
20
21 [20] Okamoto H 2008 Fe-Ge (Iron-Germanium) *J. Phase Equilibria Diffus.* **29** 1
22
23
24 [21] Hari Kumar, K.C., P. Wollants L D 1994 Thermodynamic evaluation of Fe-Sn phase
25
26
27 [22] Biswas S, Doherty J, Saladukha D, Ramasse Q, Majumdar D, Upmanyu M, Singha A,
28 Ochalski T, Morris M A and Holmes J D 2016 Non-equilibrium induction of tin in
29 germanium: Towards direct bandgap Ge_{1-x}Sn_xnanowires *Nat. Commun.* **7** 11405
30
31
32
33
34 [23] Park K H, Lee D, Kim J, Song J, Lee Y M, Kim H T and Park J K 2014 Defect-free,
35 size-tunable graphene for high-performance lithium ion battery *Nano Lett.* **14** 4306–13
36
37
38
39 [24] Biswas S, O'Regan C, Petkov N, Morris M a. and Holmes J D 2013 Manipulating the
40 growth kinetics of vapor-liquid-solid propagated ge nanowires *Nano Lett.* **13** 4044–52
41
42
43
44 [25] Meshgi M A, Biswas S, Mcnulty D, Dwyer C O, Verni G A, Connell J O, Letofsky-
45 papst I, Poelt P, Holmes J D and Marschner C 2017 Rapid, Low-Temperature Synthesis
46 of Germanium Nanowires from Oligosilylgermane Precursors
47
48
49
50
51 [26] Chan C K, Zhang X F and Cui Y 2008 High capacity Li ion battery anodes using Ge
52 nanowires *Nano Lett.* **8** 307–9
53
54
55
56 [27] Ngo D T, Kalubarme R S, Le H T T, Park C N and Park C J 2015 Conducting additive-
57
58
59
60

- 1
2
3 free amorphous GeO₂/C composite as a high capacity and long-term stability anode for
4
5 lithium ion batteries *Nanoscale* **7** 2552–60
6
7
8
9 [28] Kim G T, Kennedy T, Brandon M, Geaney H, Ryan K M, Passerini S and Appetecchi
10 G B 2017 Behavior of Germanium and Silicon Nanowire Anodes with Ionic Liquid
11 Electrolytes *ACS Nano* **11** 5933–43
12
13
14
15 [29] Forney M W, Ganter M J, Staub J W, Ridgley R D and Landi B J 2013 Prelithiation of
16 silicon-carbon nanotube anodes for lithium ion batteries by stabilized lithium metal
17 powder (SLMP) *Nano Lett.* **13** 4158–63
18
19
20
21
22
23 [30] Kennedy T, Mullane E, Geaney H, Osiak M, O'Dwyer C and Ryan K M 2014 High-
24 performance germanium nanowire-based lithium-ion battery anodes extending over
25 1000 cycles through in situ formation of a continuous porous network *Nano Lett.* **14**
26 716–23
27
28
29
30
31
32
33 [31] Qiang T, Fang J, Song Y, Ma Q, Ye M, Fang Z and Geng B 2015 Ge@C core-shell
34 nanostructures for improved anode rate performance in lithium-ion batteries *RSC Adv.*
35 **5** 17070–5
36
37
38
39
40
41 [32] Guo W, Mei L, Feng Q and Ma J 2015 Facile synthesis of Ge/C nanocomposite as
42 superior battery anode material *Mater. Chem. Phys.* **168** 6–9
43
44
45
46 [33] Choe H S, Kim S J, Kim M C, Kim D M, Lee G H, Han S B, Kwak D H and Park K W
47 2016 Synthesis of Ge/C composites as anodes using glucose as a reductant and carbon
48 source for lithium-ion batteries *RSC Adv.* **6** 72926–32
49
50
51
52
53
54 [34] Li W, Yang Z, Cheng J, Zhong X, Gu L and Yu Y 2014 Germanium nanoparticles
55 encapsulated in flexible carbon nanofibers as self-supported electrodes for high
56 performance lithium-ion batteries *Nanoscale* **6** 4532–7
57
58
59
60

- 1
2
3 [35] Fang S, Shen L, Zheng H and Zhang X 2015 Ge-graphene-carbon nanotube composite
4 anode for high performance lithium-ion batteries *J. Mater. Chem. A* **3** 1498–503
5
6
7
8 [36] Lim L Y, Fan S, Hng H H and Toney M F 2015 Storage Capacity and Cycling Stability
9 in Ge Anodes: Relationship of Anode Structure and Cycling Rate *Adv. Energy Mater.* **5**
10
11
12
13 [37] Yoon S, Park C-M and Sohn H-J 2008 Electrochemical Characterizations of
14 Germanium and Carbon-Coated Germanium Composite Anode for Lithium-Ion
15 Batteries *Electrochem. Solid-State Lett.* **11** A42
16
17
18
19
20
21 [38] Baggetto L and Notten P H L 2009 Lithium-Ion (De)Insertion Reaction of Germanium
22 Thin-Film Electrodes: An Electrochemical and In Situ XRD Study *J. Electrochem. Soc.*
23 **156** A169
24
25
26
27
28 [39] McNulty D, Geaney H, Buckley D and O'Dwyer C 2018 High capacity binder-free
29 nanocrystalline GeO₂ inverse opal anodes for Li-ion batteries with long cycle life and
30 stable cell voltage *Nano Energy* **43** 11–21
31
32
33
34
35
36 [40] Biswas S, O'Regan C, Morris M a. and Holmes J D 2015 In-situ Observations of
37 Nanoscale Effects in Germanium Nanowire Growth with Ternary Eutectic Alloys *Small*
38 **11** 103–11
39
40
41
42
43 [41] He S T, Xie S S, Yao J N, Gao H J and Pang S J 2002 Self-assembled two-dimensional
44 superlattice of Au-Ag alloy nanocrystals *Appl. Phys. Lett.* **81** 150–2
45
46
47
48
49
50
51
52
53
54
55
56
57
58
59
60

1
2
3
4
5
6
7
8
9
10
11
12
13
14
15
16
17
18
19
20
21
22
23
24
25
26
27
28
29
30
31
32
33
34
35
36
37
38
39
40
41
42
43
44
45
46
47
48
49
50
51
52
53
54
55
56
57
58
59
60

Accepted Manuscript

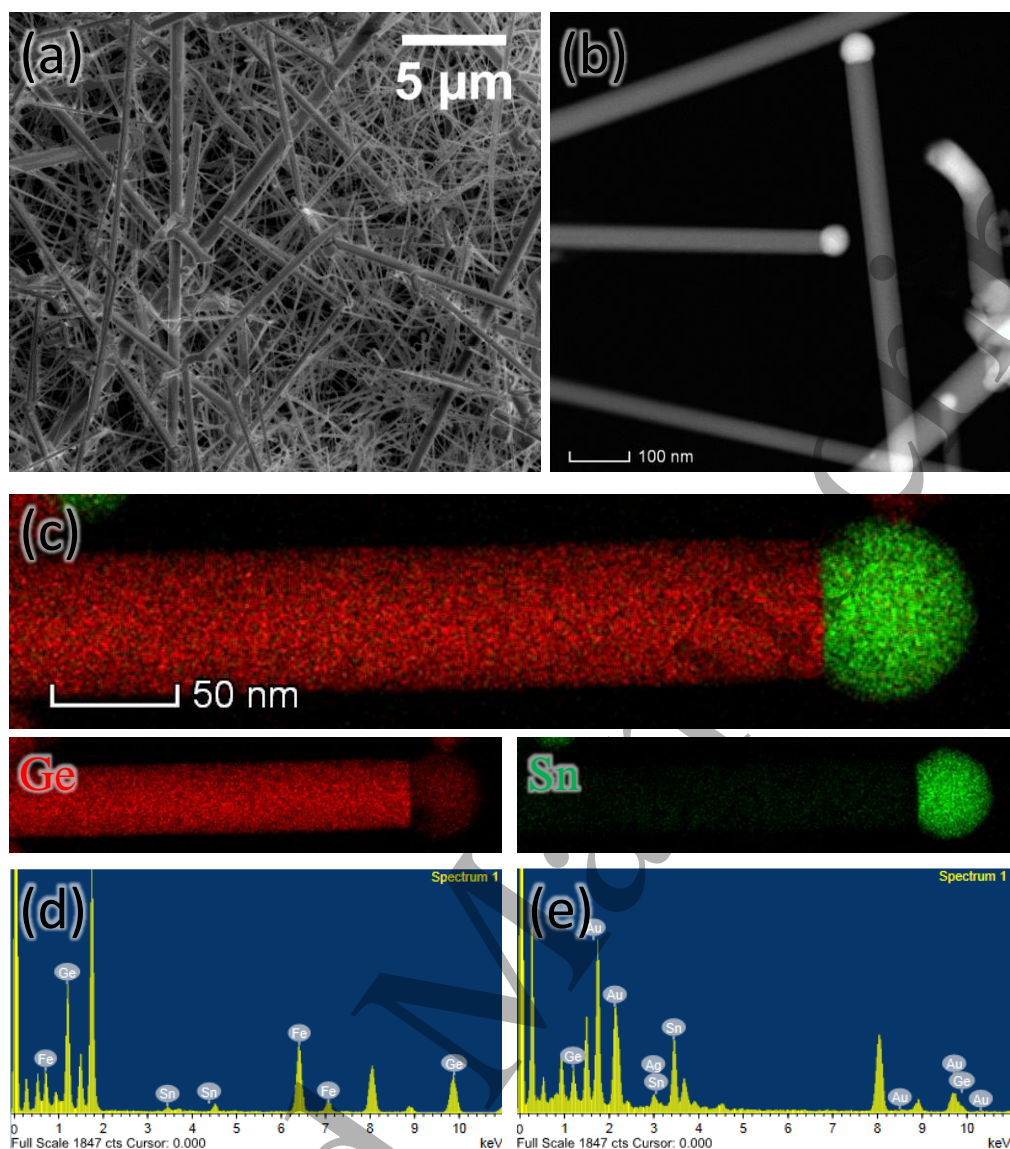


Figure 1: Structural and compositional analysis of $\text{Ge}_{1-x}\text{Sn}_x$ nanowires. SEM and STEM images of the $\text{Ge}_{1-x}\text{Sn}_x$ nanowires grown on stainless steel reveal a large variation in nanowire diameter (a) across the substrate, but a negligible change in diameter due to tapering of single nanowires (b) respectively. (c) EDX elemental mapping of $\text{Ge}_{1-x}\text{Sn}_x$ nanowires with $x = 0.048$. Ge is denoted in red and Sn in green. The nanowire in (c) is AuAg-seeded, clearly apparent from the presence of a Sn rich nanowire seed in the elemental map and therefore may have a higher than average Sn content ($x > 0.048$). Evidence of the two competing growth seeds is provided in (d) and (e), with EDX spectra displaying the presence of Fe, and Au and Ag respectively.

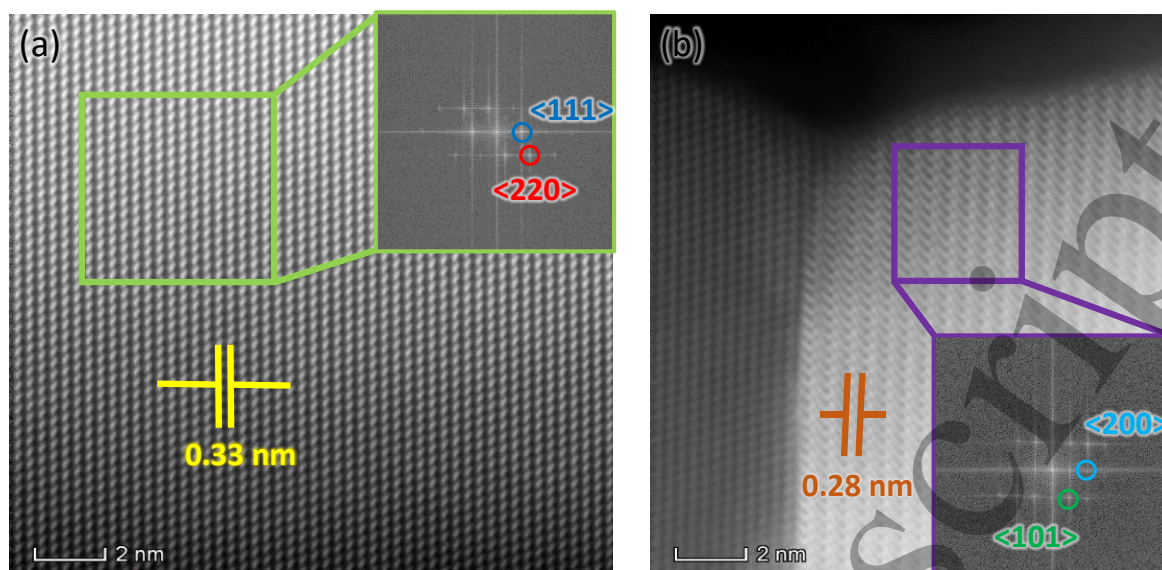


Figure 2: HAADF HRSTEM analysis of Ge_{1-x}Sn_x nanowires. (a) The Ge_{1-x}Sn_x nanowires are single crystalline with no apparent defects or twin boundaries. The lattice spacing of the nanowires is 0.33 nm, confirmed by FFT (inset). These nanowires are grown along the <111> direction. The sharp interface between the nanowire seed and body is shown in (b); FFT provided in the inset. There is negligible apparent tailing of the Sn rich seed at the growth interface.

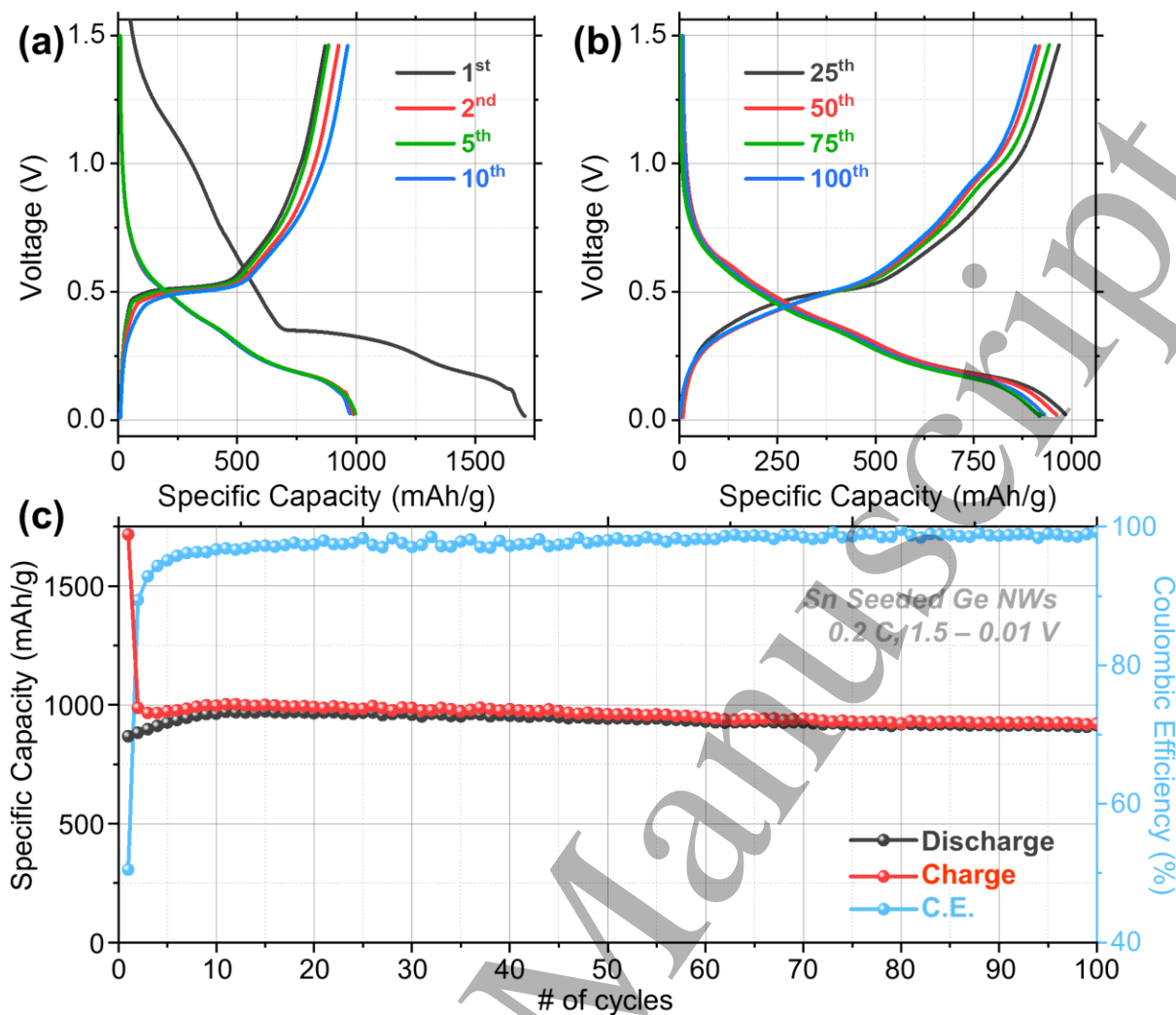


Figure 3: Electrochemical tests. Charge and discharge voltage profiles for (a) the 1st, 2nd, 5th and 10th cycles (b) the 25th, 50th, 75th and 100th cycles for Ge_{1-x}Sn_x nanowires at C/5 in a potential window of 1.5 – 0.01 V (vs Li/Li+). (c) Specific capacity and Coulombic efficiency values obtained for Ge_{1-x}Sn_x nanowires over 100 cycles.

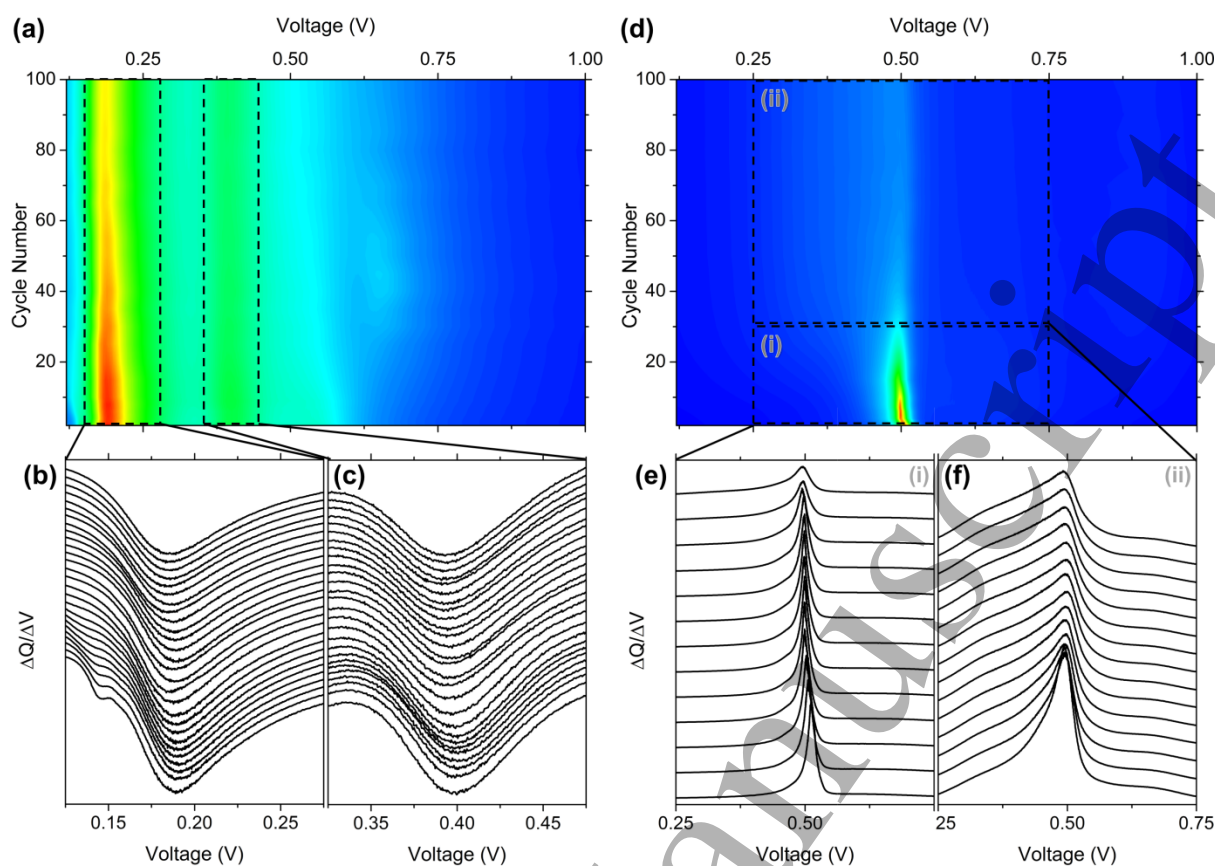


Figure 4: Differential capacity plots. (a) Differential capacity contour plot calculated from differential charge curves. Stacked differential capacity curves demonstrating the reduction peak associated with the formation of (b) the $c\text{-Li}_{15}\text{Ge}_4$ phase and (c) the $a\text{-Li}_{15}\text{Ge}_4$ phase. (d) Differential capacity contour plot calculated from differential discharge curves. Stacked differential capacity curves demonstrating the oxidation peak associated with the delithiation of for $\text{Ge}_{1-x}\text{Sn}_x$ nanowires (e) from the 1st to the 30th cycle and (f) from the 31th to the 100th cycle.